Journal for ImmunoTherapy of Cancer

Unveiling the tumor immune microenvironment of organ-specific melanoma metastatic sites

Jordan W Conway ,[1,2,3] Robert V Rawson,[1,4] Serigne Lo ,[1,2] Tasnia Ahmed,[1] Ismael A Vergara,[1,2,3] Tuba N Gide,[1,2,3] Grace Heloise Attrill ,[1,2,3] Matteo S Carlino,[1,2,5] Robyn P M Saw,[1,2,6,7] John F Thompson ,[1,2,6,7] Andrew J Spillane,[1,2,8] Kerwin F Shannon,[1,6,9] Brindha Shivalingam,[1,9] Alexander Maxwell Menzies,[1,2,7,8] James S Wilmott,[1,2,3] Georgina V Long ,[1,2,3,7,8] Richard A Scolyer ,[1,2,3,4] Ines Pires da Silva [1,2,3,5]

To cite: Conway JW, Rawson RV, Lo S, *et al*. Unveiling the tumor immune microenvironment of organ-specific melanoma metastatic sites. *Journal for ImmunoTherapy of Cancer* 2022;**10**:e004884. doi:10.1136/jitc-2022-004884

► Additional supplemental material is published online only. To view, please visit the journal online (http://dx.doi.org/10.1136/jitc-2022-004884).

GVL, RAS and IPdS contributed equally.

Accepted 24 August 2022

For numbered affiliations see end of article.

Correspondence to
Dr Ines Pires da Silva;
Ines.Silva@melanoma.org.au

ABSTRACT

Background The liver is a known site of resistance to immunotherapy and the presence of liver metastases is associated with shorter progression-free and overall survival (OS) in melanoma, while lung metastases have been associated with a more favorable outcome. There are limited data available regarding the immune microenvironment at different anatomical sites of melanoma metastases. This study sought to characterize and compare the tumor immune microenvironment of liver, brain, lung, subcutaneous (subcut) as well as lymph node (LN) melanoma metastases.

Methods We analyzed OS in 1924 systemic treatment-naïve patients with AJCC (American Joint Committee on Cancer) stage IV melanoma with a solitary site of organ metastasis. In an independent cohort we analyzed and compared immune cell densities, subpopulations and spatial distribution in tissue from liver, lung, brain, LN or subcut sites from 130 patients with stage IV melanoma.

Results Patients with only liver, brain or bone metastases had shorter OS compared to those with lung, LN or subcutaneous and soft tissue metastases. Liver and brain metastases had significantly lower T-cell infiltration than lung (p=0.0116 and p=0.0252, respectively) and LN metastases (p=0.0116 and p=0.0252, respectively). T cells were further away from melanoma cells in liver than lung metastases (p=0.0335). Liver metastases displayed unique T-cell profiles, with a significantly lower proportion of programmed cell death protein-1+ T cells compared to all other anatomical sites (p<0.05), and a higher proportion of TIM-3+ T cells compared to LN (p=0.0004), subcut (p=0.0082) and brain (p=0.0128) metastases. Brain metastases had a lower macrophage density than subcut (p=0.0105), liver (p=0.0095) and lung (p<0.0001) metastases. Lung metastases had the highest proportion of programmed death ligand-1+ macrophages of the total macrophage population, significantly higher than brain (p<0.0001) and liver metastases (p=0.0392).

Conclusions Liver and brain melanoma metastases have a significantly reduced immune infiltrate than lung, subcut and LN metastases, which may account for poorer prognosis and reduced immunotherapy response rates in patients with liver or brain metastases. Increased TIM-3 expression in liver metastases suggests TIM-3 inhibitor therapy as a potential therapeutic opportunity to improve patient outcomes.

WHAT IS ALREADY KNOWN ON THIS TOPIC

⇒ Although immune checkpoint inhibitors (ICI) have increased response and survival rates in metastatic melanoma, many patients will be resistant to these therapies. The presence or absence of specific sites of metastasis has been associated with differences in response and survival rates to ICI. The biology underlying these differences however is unknown.

WHAT THIS STUDY ADDS

⇒ Different sites of melanoma metastasis harbor distinct tumor immune microenvironments characterized by differences in T cell and myeloid immune cell populations and their spatial distribution. While liver metastases were shown to have reduced CD3+ T-cell density, reduced programmed cell death protein-1 (PD-1) expression and increased Tim-3 expression, lung and lymph node metastases had an increased density of CD3+ T cells and PD-1 expression.

HOW THIS STUDY MIGHT AFFECT RESEARCH, PRACTICE OR POLICY

⇒ This study provides insights into the biology of melanoma metastases at different sites, and highlights potential organ-specific drug targets.

INTRODUCTION

Immunotherapy, specifically with immune checkpoint inhibitors (ICI), has become the standard treatment for patients with high-risk early-stage and advanced-stage melanoma,[1–5] small cell and non-small cell lung cancer,[6–8] and several other solid tumor malignancies.[9] ICI have produced significant improvement of clinical outcomes in advanced melanoma, with 5-year overall survival (OS) of 44% and 52% for anti-programmed cell death protein-1

(PD-1) monotherapy and combined anti-PD-1 plus anti-cytotoxic T-lymphocytes-associated protein 4 (CTLA-4), respectively.[10] Use of adjuvant ICI have also resulted in an improvement in the recurrence-free survival of patients with high-risk resectable stage III melanoma and have become standard of care in these patients.[1 2]

While ICI therapies have significantly improved patient outcomes, approximately 40–55% of patients with advanced melanoma have primary resistance to ICI and up to 43% of patients who initially respond develop acquired resistance during the course of their treatment.[11–13] These data highlight the need for better understanding of the biology associated with the immune response to ICI, and how the tumor immune microenvironment (TIME) influences this response. Several studies have identified factors associated with response and resistance to ICI. While high expression of programmed death ligand-1 (PD-L1), high tumor mutational burden, high interferon-gamma expression and increased tumor CD8+ T-cell density are associated with better responses to ICI,[14–17] elevated baseline lactate dehydrogenase (LDH) levels have been associated with shorter OS in patients with melanoma treated with anti-PD-1 alone or in combination with anti-CTLA-4.[10 18] More recent studies have indicated that the anatomical site of metastasis in patients with advanced melanoma is associated with ICI response and overall prognosis, suggesting potential site-specific mechanisms of response or resistance to current ICI therapies. For example, the presence of lung metastases has been associated with increased response rates and longer progression-free survival (PFS), whereas liver metastases have poorer responses and are associated with shorter survival rates when treated with either anti-PD-1 monotherapy or in combination with anti-CTLA-4 therapy in patients with advanced lung cancer and melanoma, respectively.[19 20]

Further characterization and investigation of the TIME at different anatomical sites of metastasis is needed to better understand possible mechanisms of response and resistance in patients to anti-PD-1-based therapies. In this study, we sought to characterize and compare the TIME in untreated melanoma metastases from five different anatomical sites.

MATERIALS AND METHODS

Patient study cohort

The Melanoma Institute Australia (MIA) research database (MRD) was used to identify two cohorts of patients: (1) cohort 1, included systemic treatment-naïve patients with AJCC (American Joint Committee on Cancer) stage IV melanoma who developed only a solitary site of organ metastasis and never received subsequent systemic therapy (n=1924); and (2) cohort 2, included systemic treatment-naïve patients with stage IV melanoma who had available formalin-fixed paraffin-embedded (FFPE) samples between 1993 and 2017 from at least one target site of interest (n=130). Patients from cohort 2 may have had or developed other sites of metastases. A total of 137 biopsies (core n=11; excisional n=126) were included (liver (n=20), brain (n=38), lung (n=24), lymph nodes (LN; n=38) and subcutaneous (subcut; n=17)); seven patients had two lesions from separate sites included in the study. A subset of patients from cohort 2 (n=35) received anti-PD-1-based systemic therapy after the sample was obtained. We have included an additional 32 patients with stage IV melanoma treated with anti-PD-1-based immunotherapy who had available baseline melanoma tissue samples in order to increase the sample size for the comparison of the tumor microenvironment (T cell panel) between responders versus non-responders. Patients with mucosal, uveal or acral primary melanoma were excluded from the study. Samples were obtained from patients consented at Poche Centre MIA, Royal Prince Alfred Hospital and Westmead Hospital. Informed patient consent was obtained through the MIA Biospecimen bank for specimen use and for access to clinical data from the MIA MRD.

Pathological assessment

H&E-stained sections were assessed by a pathologist to confirm melanoma content. Specimens that did not meet minimal tissue requirements for assessment (<10% tumor content or <100 tumor cells) were excluded from analysis (n=8). Tumor-infiltrating lymphocyte (TIL) density was scored on a semi-quantitative scale (0–3), 0 being no TILs present and 3 representing high TIL density. Percentage of tumor involvement with TILs was also assessed. Samples were given a non-conventional TIL score calculated as TIL density score (0–3) × per cent of tumor involvement with TILs (0–100%) out of a maximum score of 300 as adapted from methods described previously.[21] Other immune inflammatory cells, intratumoral fibrosis and necrosis was also noted.

Opal multiplex immunofluorescence

The 3 µm FFPE sections were mounted on positively-charged Superfrost Plus slides (Thermo Fisher Scientific) and dried before being placed in an oven at 65°C for 30–60 min. Sections were then deparaffinized in xylene followed by decreasing graded concentrations of ethanol and rinsed in TBST (Tris-buffered saline + Tween20). Antigen retrieval was performed using pH9 or pH6 buffer (Akoya Biosciences) as required in a decloaking chamber (Biocare Medical) heated to 110°C for 10 min. Subsequent staining was performed on an automated slide staining system (Intellipath FLX, Biocare Medical). Slides were blocked with 3% H_2O_2 (Sigma-Aldrich) for 10 min to block endogenous horseradish peroxidase (HRP) activity. Two multiplex panels (online supplemental tables 1,2) were then stained targeting (1) PD-1 (Abcam, 1:400), CD103 (Abcam, 1:1500), FoxP3 (Abcam, 1:2000), TIM-3 (Cell Signaling Technology, 1:500), CD3 (Cell Marque, 1:2000), and SOX10 (Biocare Medical, 1:200), or (2) CD14 (Cell Marque, 1:100), PD-L1 (Cell Signaling Technology, 1:1000), CD68 (Cell Marque, 1:500), CD16a

(Cell Marque, 1:400), and SOX10 (Biocare Medical, 1:200) incubating for 30 min or 45 mins (TIM-3). Detection of primary antibody was achieved using MACH3 HRP-polymer detection kit (CD14) for 10 min, or Opal HRP conjugated polymer (anti-mouse/anti-rabbit, PerkinElmer) for 30 min. Visualization was achieved through Opal tyramide signal amplification (Akoya Biosciences) for 10 min. Between each subsequent staining run slides were stripped via heat treating in appropriate pH buffer for 10 min at 110°C. Following the final staining run, samples were stained with spectral DAPI (Akoya Biosciences), coverslipped using ProLong Diamond Antifade Mountant (Thermo Fisher) and left to dry overnight at room temperature away from light exposure. Positive and negative control slides were also included in each staining batch.

Fluorescent image analysis

The Vectra V.3.0 automated quantitative pathology imaging platform along with Vectra V.3.3 and Phenochart V.1.0.12 software (Akoya Biosciences) was used to scan whole tissue slides and obtain multispectral images of each sample. Spectral unmixing of images was achieved through inForm V.2.4.8 software (Akoya Biosciences) using a spectral library created from each of the individual fluorophores used. Quantitative image analysis was performed using the using HALO software V.3.0.1 (Indica Labs). The algorithm was trained to classify regions of tissue into tumor versus stroma based on the expression of DAPI and SOX10. Therefore, when analyzing intratumoral immune cell densities, stromal tissue regions were excluded from analysis. Cell segmentation was performed by watershed to identify cellular expression of protein markers. The threshold of protein expression of each marker was determined for each batch with positive and negative control slides used to compensate for any batch variation. Data was exported as single cell data for secondary analysis. TIBCO Spotfire V.7.11.1 software was used for quantitative analysis and cell phenotyping. Phenotyped cell densities were calculated as the number of cells positive for a particular marker divided by tumor area for the sample (cells per mm^2). Spatial analysis was performed using HALO V.3.0.1 (Indica Labs). Spatial plots were generated for select phenotypes. Average distances between melanoma cells and immune cells were analyzed using the software's proximity analysis settings and the densities of immune cells within 20 µm of melanoma cells were calculated.

Statistical analysis

The Mann-Whitney U test and the Kruskal-Wallis test were used for testing the median difference between two groups and more than two groups, respectively. For data comparing more than two groups, false discovery rate was controlled for and p values adjusted using the Benjamini and Hochberg procedure. Survival outcomes were described using the Kaplan-Meier method. The logrank test was used to test the difference between survival curves. Associations of each factor with OS and PFS were assessed from univariable Cox proportional hazards (Cox PH) models. Factors for which the HRs were statistically significant at the 0.05 significance level were included in a multivariable Cox PH model. A p value of less than 0.05 was considered statistically significant. All graphical data included the median with 95% CI. Statistical analysis and graphs were generated using GraphPad Prism V.8.2, SAS V.9.4 (SAS Institute, Cary, North Carolina, USA) and R V.3.6.3 (R Foundation for Statistical Computing, Vienna, Austria).

RESULTS

Patients with liver, brain and bone metastases as the only site of disease had shorter survival compared with other sites of disease

From the MIA research database, we identified 1924 patients with stage IV melanoma with no exposure to systemic treatment (24% had radiotherapy and 28% had surgery) and with only one site of distant metastasis distributed as follows: brain (n=479; 25%), lung (n=562; 29%), liver (n=272; 14%), gastrointestinal (any organ from the gastrointestinal tract; n=63; 3%), bone (n=151; 8%), subcutaneous and soft tissue (S&S) (n=233; 12%) and LN (n=164; 9%). Median age was 62 years (range 18–96) and 65% of patients (n=1245) were men. Patients with only liver (median overall survival (mOS) 3.9 months), brain (mOS 4.0 months) or bone (mOS 4.8 months) metastases had shorter OS compared with those with lung (mOS 9.6 months), LN (mOS 13.6 months) or S&S metastases (mOS 14 months) (p<0.0001; figure 1; online supplemental table 3). Multivariable analysis including age, gender, sites of disease, number of metastases and LDH, found that brain, liver and bone metastases were still independent poor prognostic features (online supplemental tables 4,5).

To identify why there was a significant difference in OS for patients with different sites of metastasis and, more specifically, why patients with only liver or brain metastases have shorter survival compared with patients with only lung, LN or S&S metastases, we studied 137 melanoma biopsies collected from 130 patients and from five anatomical sites: liver (n=20), brain (n=38), LN (n=38), lung (n=24) and subcut (n=17) (online supplemental table 6). Only 35 patients (26%) had received anti-PD-1-based therapy after the tumor sample had been procured (online supplemental table 7), and the presence of brain and liver metastases was associated with numerically shorter PFS and OS, supporting previous data published by us and others[19 22] (online supplemental figures 1–4, tables 8,9).

Liver metastases had the lowest TIL score and brain metastases had the lowest levels of fibrosis compared with other anatomical sites

TIL score was compared across anatomical sites of metastases based on H&E-stained sections (figure 2A,B; online

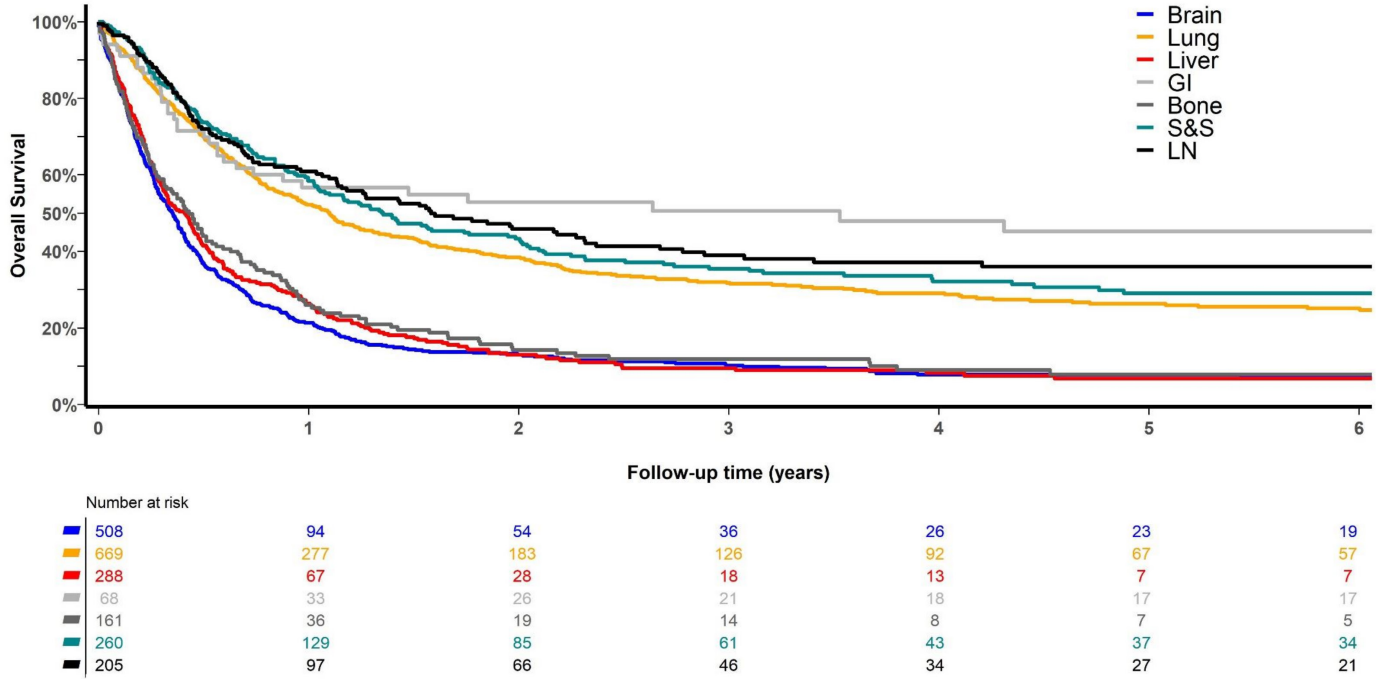

Figure 1 Kaplan-Meier curve showing the overall survival of patients with only one organ-site of metastasis, who had no systemic therapy. Comparison was made between patients who had brain (*blue; n=479*), lung (*yellow; n=562*), liver (*red; n=272*), gastrointestinal (GI; *light gray; n=63*), bone (*dark gray; n=151*), subcutaneous and soft tissue (S&S; *green; n=233*) and lymph node (LN; *black; n=164*) as the only organ-site of metastases. Number of patients at risk at baseline, 1, 2, 3, 4, 5 and 6 years are presented.

supplemental table 10). Lung and LN metastases had the highest TIL scores (medians=80 and 60, respectively) while liver, brain and subcut metastases had lower scores (medians=30, 30, and 20, respectively). While there was a significant difference when comparing TIL scores across all anatomical sites (p=0.0203), these results did not reach significance on pairwise comparisons. Brain metastases had the highest level of necrosis (median=10%) however there was no significant difference in the percentage of necrosis across the five anatomical sites (figure 2A,C). On the contrary, brain and lung metastases had lower levels of fibrosis compared with liver (p=<0.0001 and p=0.0466, respectively) and to subcut (p=<0.0001 and p=0.0055, respectively) metastases (figure 2A,D).

Liver and brain metastases had reduced CD3+ T-cell infiltration but brain metastases expressed the highest proportion of PD-1+ T cells across the five anatomical sites

We next sought to further characterize the TIME at each anatomical site of metastasis using multiplex immunofluorescence (figure 3A,B). First, we examined the density of CD3+ T cells within each tumor and compared across the five sites of metastasis (figure 3C, online supplemental figure 5). CD3+ T-cell density was significantly lower in liver (median=154 cells/mm^2) and brain metastases (median=181 cells/mm^2) compared with lung (436 cells/mm^2; p=0.0116 and p=0.0252, respectively) and LN metastases (median=467 cells/mm^2; p values, p=0.0116 and p=0.0252, respectively). Subcut metastases also had a significantly lower CD3+ T cell density (median=221 cells/mm^2) compared with lung and LN metastases (p=0.0389 and p=0.0389, respectively), although to a lesser extent than brain and liver metastases.

We then examined T cell subsets expressing CD103, TIM-3, PD-1 and FoxP3 and their proportion of the total CD3+ T-cell population (figure 3A,D–G). Liver metastases had the lowest proportion of PD-1+ T cells (median=0.7%) compared with brain (median=8.9%), subcut (median=7.2%), lung (median=3.2%) and LN (median=4.8%) metastases (p<0.05) (figure 3D). Notably, brain metastases had the highest overall proportion of CD3+ T cells expressing PD-1 and was significantly higher than liver and LN metastases (p=0.0342). In contrast, the proportion of CD3+ T cells expressing TIM-3 was significantly higher in liver (median=10.7%) and lung metastases (median=12.9%) compared with brain (median=3.3%), subcut (median=2.9%) and LN metastases (median=0.9%) (p<0.01) (figure 3E). CD103, a tissue-residency marker, was also compared across the five anatomical sites (figure 3F). Notably, brain metastases had the lowest proportion of CD103+ T cells (median=2.6%) compared with all other metastatic sites (p<0.05), while subcut and lung metastases had the highest proportion of CD103+ T cells (medians=14.1% and 12.6%, respectively). Finally, subcut (median=3.7%) and LN metastases (median=3.4%) had the highest proportion of FoxP3+ T cells among the five anatomical sites of metastasis (p≤0.001) (figure 3G). Of note, 38% of brain metastases (15/40) lacked FoxP3+CD3+ T cells.

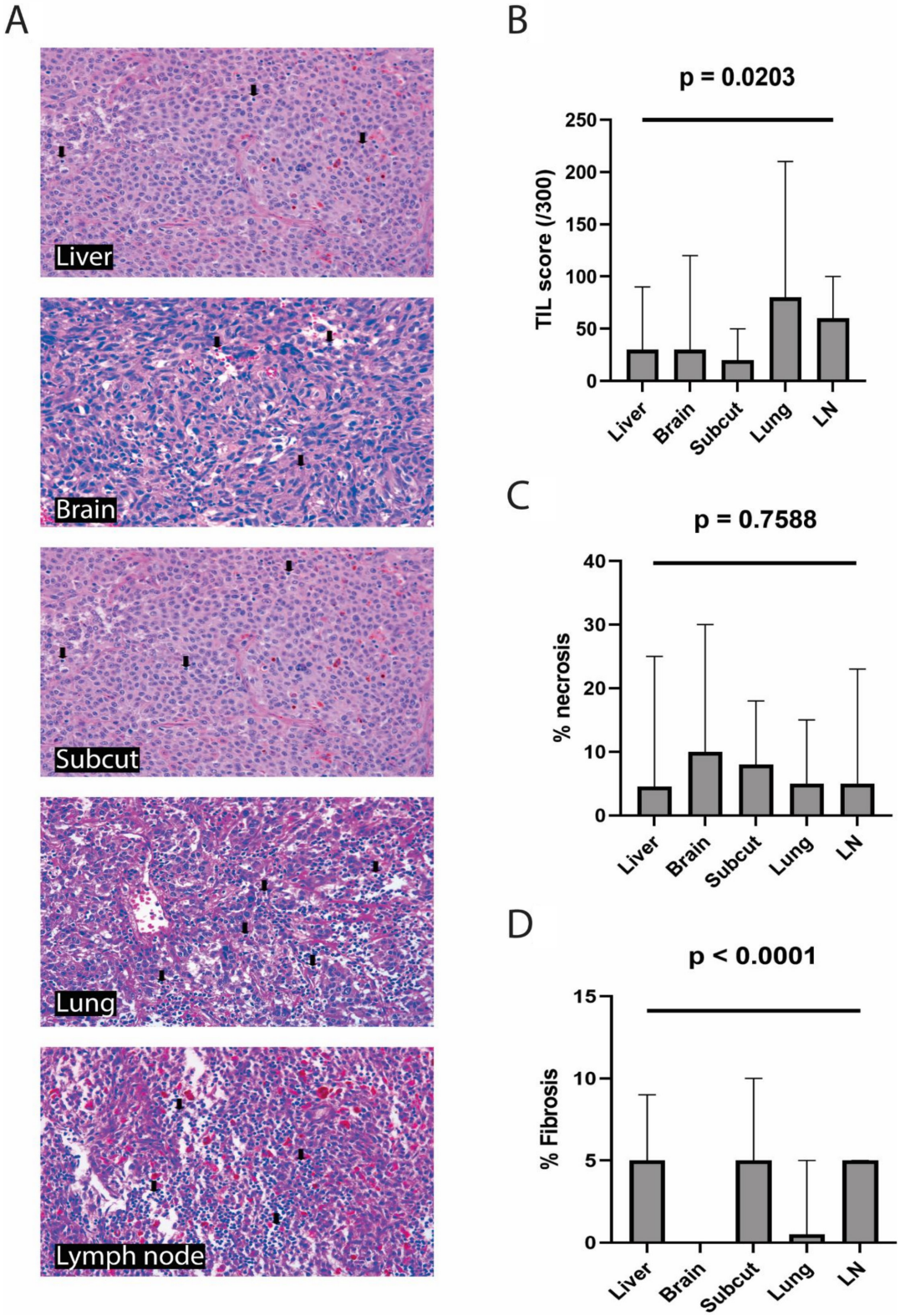

Figure 2 Comparison of routine histological characteristics across different anatomical sites of melanoma metastasis. (A) Representative images showing H&E-stained sections of a liver, brain, subcutaneous (subcut), lung and lymph node (LN) metastasis with black arrows noting lymphocytes. (B) Comparison of tumor-infiltrating lymphocyte (TIL) score (TIL density × percentage of tumor infiltrated by lymphocytes) out of a maximum score of 300 between these five anatomical sites of metastases. (C) Comparison of percentage of tumor tissue exhibiting necrosis between these five anatomical sites of metastases. (D) Comparison of percentage of tumor tissue exhibiting fibrosis between these five anatomical sites of metastases. Pairwise comparison liver versus brain and lung ($p<0.0001$ and $p=0.0466$, respectively). Subcut versus brain and lung ($p<0.0001$ and $p=0.0055$, respectively). Error bars represent median with 95% CI. Figure p values of the comparison across all anatomical sites were presented (Kruskal-Wallis p value).

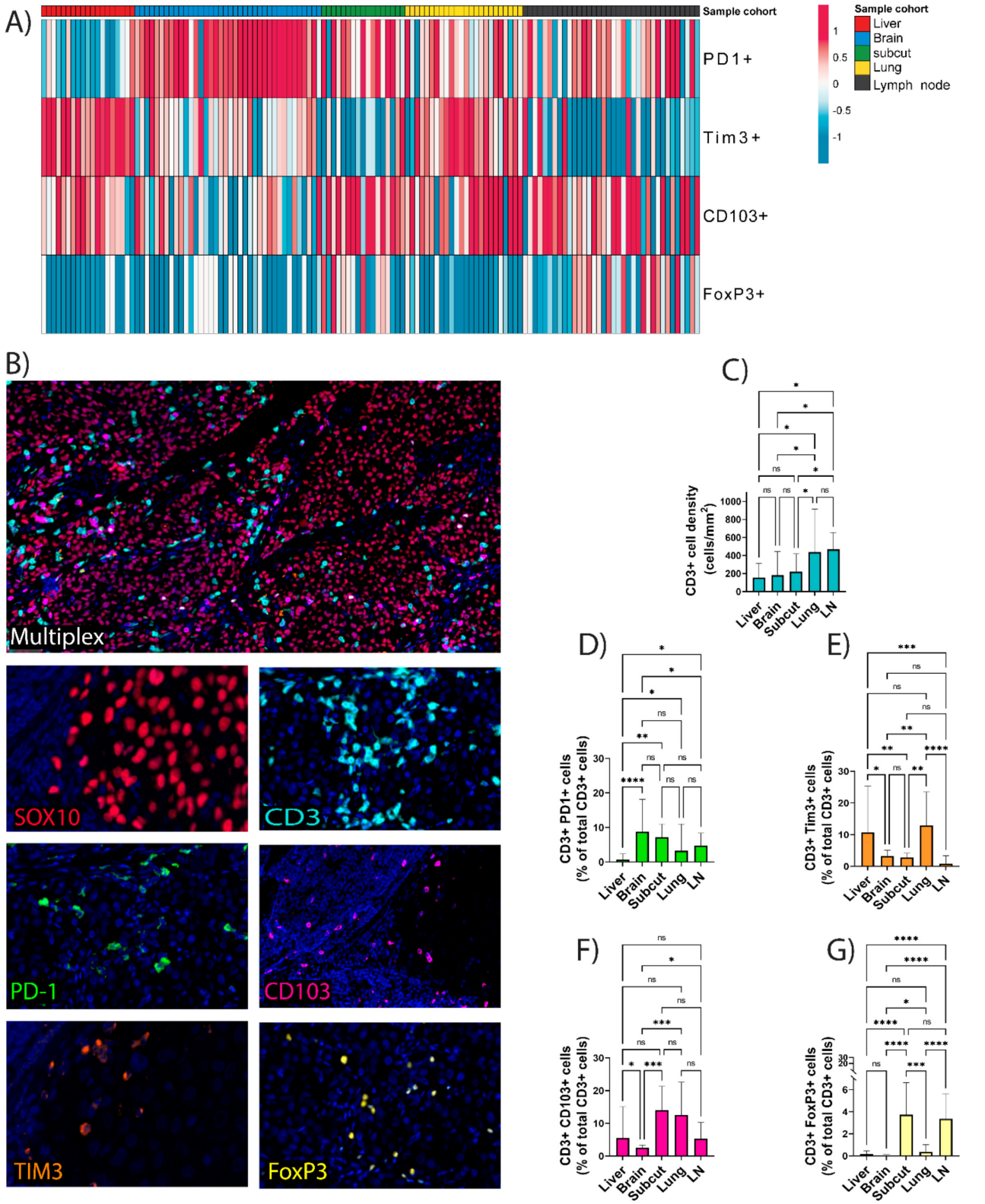

Figure 3 Comparison of T cell populations across five anatomical sites of melanoma metastasis. (A) Heatmap illustrating the comparison of T cell subpopulation proportions between cohorts based on IHC data. Columns represent patients (liver (*red*); brain (*blue*); subcutaneous (subcut; *green*); lung (*yellow*) and LN (lymph nodes; *black*)) and rows the IHC marker. Unit variance scaling applied where higher proportion indicated by positive values (red) and lower proportion indicated by negative values (blue). (B) Representative multiplex immunohistochemistry images of SOX10, CD3, FoxP3, PD-1, CD103, and TIM-3 in melanoma tissue. (C) Comparison of the CD3+ T cell density (cells/mm^2) and the proportion of CD3+ T cells co-expressing (D) PD-1, (E) TIM-3, (F) CD103 and (G) FoxP3 between five different sites of melanoma metastasis, liver, brain, subcutaneous, lung and lymph nodes. Error bars represent median with 95% CI. *p<0.05, **p<0.01, ***p<0.001, ****p<0.0001. IHC, immunohistochemistry; ns, non-significant.

CD3+ T cells were closest to melanoma cells in lung metastases compared with other sites, and liver metastases had the highest proportion of TIM-3+ T cells in close proximity to melanoma cells

With research highlighting the importance of spatial proximity between tumor cells and immune cells,[23] we analyzed the average distance between SOX10+ melanoma cells and CD3+ T cells within the tumor microenvironment (figure 4A). As expected, this distance negatively correlated with CD3+ T cell density (online supplemental figure 6). CD3+ T cells were closer to melanoma cells within the lung (median=57 µm) compared with liver (median=83 µm), brain (median=98 µm) and subcut (median=134 µm) metastases (p<0.05) (figure 4B). Further, we assessed the density of CD3+ T cells in close proximity (≤20 µm) to a melanoma cell (figure 4C). Lung metastases had the highest density of CD3+ T cells within 20 µm of a melanoma cell (median=282 cells/mm^2), particularly compared with liver (median=123 cells/mm^2), subcut (median=102 cells/mm^2) and brain (median=78 cells/mm^2) metastases (p<0.05).

We then analyzed the proportion of T cells expressing PD-1, TIM-3, CD103 and FoxP3 within 20 µm of a melanoma cell at each metastatic site (figure 4D). In agreement with the result obtained above when assessing the total tumor microenvironment, brain metastases had the highest percentage of PD-1+ T cells within 20 µm of a melanoma cell (median=11.2%) particularly compared with liver metastases (median=2%; p=0.0179) and to a lesser extent to LN metastases (median=5.0%; p=0.0227) (online supplemental figure 7). In addition, the proportion of TIM-3+ T cells within 20 µm of a melanoma cell was higher in liver (median=18.6%) and lung (median=14.5%) metastases versus brain, subcut and LN metastases (p≤0.001). Within the liver metastases, unlike within lung metastases, there was a significantly higher proportion of TIM-3+ T cells versus PD-1+ T cells (18.6% vs 2%) within 20 µm of a melanoma cell (p=0.0124). In contrast, brain metastases showed a significantly lower proportion of TIM-3+ T cells compared with PD-1+ T cells (3.1% vs 11.2%; p=0.0013). Similar to the above findings in the overall tumor environment, the proportion of CD103+ T cells within 20 µm of a melanoma cell was higher in subcut (median=14.6%) and lung (median=14.7%) metastases compared with the other metastatic sites, in particular compared with brain metastases (median=3.1%; p=0.0019 and p=0.0002, respectively). The proportion of FoxP3+ T cells within 20 µm of a melanoma cell was low at all metastatic sites, with no differences observed across them.

CD68+ macrophage densities were highest in lung and liver metastases compared with other sites, and had the highest PD-L1 expression in lung metastases

We next sought to evaluate myeloid-derived cells, specifically CD68+ macrophages, and compared these cells across the five anatomical metastatic sites (figure 5A,B, online supplemental figure 8). The density of CD68+ macrophages in brain metastases (median=33 cells/mm^2) was significantly lower than liver (median=290 cells/mm^2; p=0.0095), subcut (median=154 cells/mm^2; p=0.0105) and lung metastases (median=372 cells/mm^2; p<0.0001); lung metastases displayed the highest CD68+ macrophage density across all sites (figure 5C). We also sought to determine whether CD68+ density correlated with CD3+ T cell density across the sites of disease. We observed significant positive correlations within the liver (Spearman's r=0.53, p=0.0252), subcut (Spearman's r=0.68, p=0.0012) and LN (Spearman's r=0.50, p=0.0034) metastases, but not in lung or brain metastases (online supplemental figure 9).

We then examined macrophage subsets expressing CD16, CD14 and PD-L1 and their proportion of the total CD68+ macrophage population (figure 5A,D–G). The majority (>60%) of CD68+ macrophages co-expressed CD16 across the five anatomical sites of metastases and on pairwise comparison there was no significant difference between sites (figure 5D). The lowest proportion of CD14+ macrophages was observed in the brain metastases (median=7.15%) and was significantly lower than at all other sites in this study (p<0.01) (figure 5E). The proportion of CD68+ macrophages expressing PD-L1 was highest in lung metastases (median=18.73%); significantly higher than in brain (median=0.65%; p<0.0001) and liver (median=5.2%; p=0.0392) metastases. Brain metastases had the lowest proportion of PD-L1+ macrophages compared with all other anatomical sites (p<0.01) (figure 5F). As PD-L1 expression on tumor cells is strongly associated with response to anti-PD-1 therapy across many cancers, and is used to select therapy in non-small cell lung cancer (NSCLC), we also analyzed the proportion of SOX10+ melanoma cells expressing PD-L1 (figure 5G). Similar to the level of expression on CD68+ macrophages, brain had the lowest expression of PD-L1 on SOX10+ melanoma cells (median=0.03%) while the lung had the highest proportion (median=4.3%) compared with the brain (p=<0.0001) and the LN metastases (median=0.25%; p=0.005).

CD68+ macrophages were furthest away from melanoma cells in brain metastases, but closer in lung and liver metastases

We analyzed the spatial distribution of the CD68+ macrophages and the relative proximities of CD68+ macrophages to melanoma cells. CD68+ macrophages were on average furthest away from melanoma cells in brain metastases (median=464 µm) and, as a result, had the lowest density of CD68+ macrophages within 20 µm of a melanoma cell (median=16 cells/mm^2) compared with all other sites (p<0.05) (figure 6A,B). On the other hand, in lung and liver metastases CD68+ macrophages were closer to melanoma cells (median=47 µm and median 53 µm, respectively), and subsequently had the highest density of CD68+ macrophages within 20 µm of a melanoma cell (median=395 cells/mm^2 and 210 cells/mm^2, respectively) (figure 6A,B).

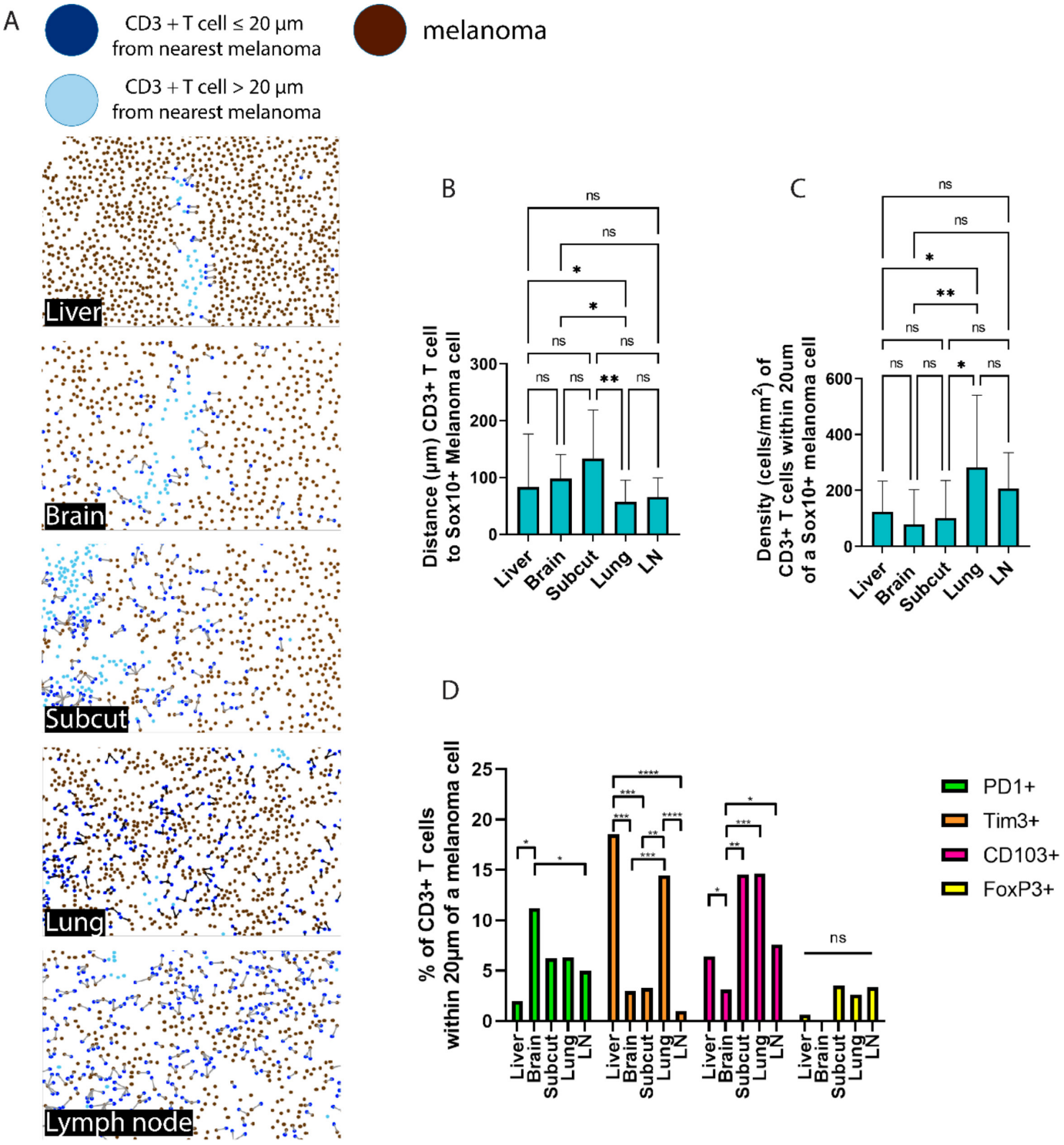

Figure 4 Spatial proximity analysis of T cell populations comparing different metastatic sites. (A) Representative images of the spatial proximity analysis mask for each site of metastasis. (B) Metastatic site (liver, brain, subcutaneous (subcut), lung and lymph node (LN)) comparison of the average distance from CD3+ T cells to Sox10+ melanoma cells. (C) Comparison of density (cells per mm^2 of tumor) of CD3+ T cells within 20 µm of an Sox10+ melanoma cell in liver, brain, subcut, lung and LN metastases. (D) Proportion (%) of CD3+ T cells expressing PD-1, TIM-3, CD103 and FoxP3 within 20 µm of an Sox10+ melanoma cell across different metastatic sites (liver, brain, subcut, lung and LN). Error bars represent median with 95% CI. *p<0.05, **p<0.01, ***p<0.001, ****p<0.0001, ns, non-significant.

As we did for the T-cell analysis, we then examined the proportions of the CD68+ macrophage subpopulations within 20 µm of a melanoma cell to compare between sites (figure 6C). As described previously, the majority of CD68+ macrophages (>60%) also expressed CD16+, and no significant differences were observed in the proportions of CD16+ macrophages between sites (figure 6D). Brain metastases had the lowest proportion

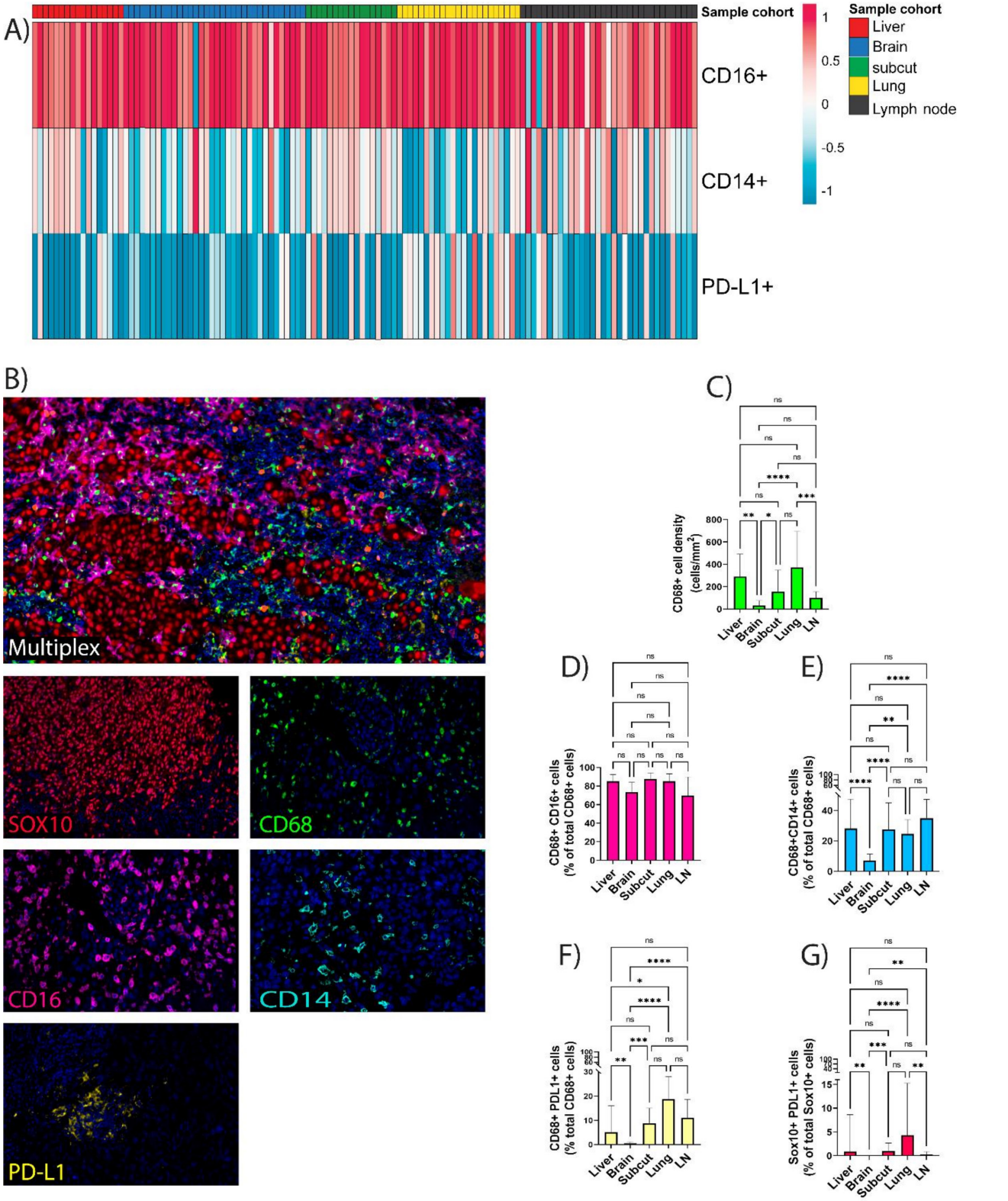

Figure 5 Comparison of macrophage populations between sites of melanoma metastasis. (A) Heatmap illustrating the comparison of CD68+ myeloid subpopulation proportions between cohorts based on IHC data. Columns represent patients (liver (*red*); brain (*blue*); subcutaneous (subcut; *green*); lung (*yellow*) and LN (lymph nodes; *black*)) and rows the IHC marker. Unit variance scaling applied where higher proportion indicated by positive values (red) and lower proportion indicated by negative values (blue). (B) Representative multiplex immunohistochemistry images of SOX10, CD16, PD-L1, CD68, and CD14 in melanoma tissue. (C) Comparison of the CD68+ macrophage density (cells/mm^2) and the proportion of CD68+ macrophages expressing (D) CD16, (E) CD14, and (F) PD-L1 in liver, brain, subcut, LN metastases. (G) Comparison of the proportion of SOX10+ melanoma cells expressing PD-L1 between sites of metastasis. Error bars represent median with 95% CI. *p<0.05, **p<0.01, ***p<0.001, ****p<0.0001. IHC, immunohistochemistry; ns, non-significant.

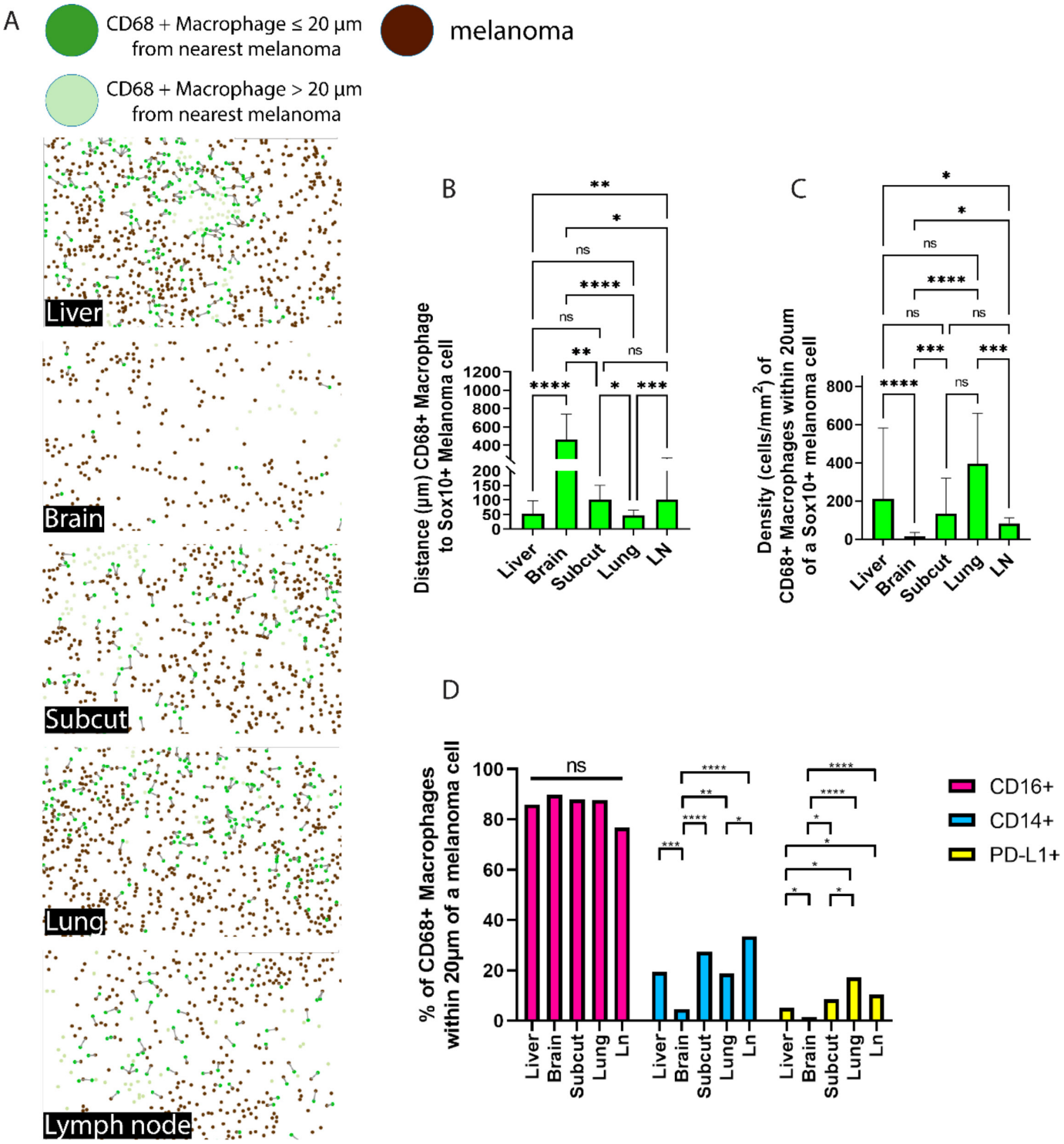

Figure 6 Spatial proximity analysis comparing myeloid populations between metastatic sites. (A) Representative images of the spatial proximity analysis mask for each site of metastasis. (B) Metastatic site (liver, brain, subcutaneous (subcut), lung and lymph node (LN)) comparison of the average distance from CD68+ macrophages to Sox10+ melanoma cells. (C) Comparison of density (cells per mm^2 of tumor) of CD68+ macrophages within 20 µm of an Sox10+ melanoma cell in liver, brain, subcut, lung and LN metastases. (D) Proportion (%) of CD68+ macrophages expressing CD16, CD14 and PD-L1 within 20 µm of an Sox10+ melanoma cell across different metastatic sites (liver, brain, subcut, lung and LN). Error bars represent median with 95% CI. *p<0.05, **p<0.01, ***p<0.001, ****p<0.0001, ns, non-significant.

of CD14+ macrophages within 20 µm of a melanoma cell (median=4.7%), which was significantly lower compared with all other anatomical sites (p<0.0001). Brain metastases also had the lowest proportion of PD-L1+ macrophages (median=1.3%), which was significantly lower than all other metastatic sites in this study (p<0.05), while lung had the highest proportion of PD-L1+ macrophages within 20 µm of a melanoma cell (median=17.2%). When

comparing the relative proportion of each macrophage subpopulation within 20 µm of a melanoma cell, all anatomical sites displayed the same pattern, with CD16+ macrophages being the dominant population in all sites (online supplemental figure 10).

With 35 patients included in cohort 2 having received subsequent anti-PD-1-based immunotherapy, we sought to assess if any trends were observed when comparing immune cell infiltrates between 'responders' versus 'non-responders' for each site.

In order to increase the sample size, we have included 32 additional patients also treated with anti-PD-1-based immunotherapy. From these, we have compared brain metastases (brain 'non-responders' vs brain responders) and lung metastases (lung 'non-responders' vs lung 'responders') in the analysis, as there was an insufficient number of liver, subcut or LN samples from treated patients to assess. Limited by small numbers, we observed non-significant trends towards a lower proportion of CD3+ T cells, but higher proportion of exhausted (PD1+ and TIM-3+) resident (CD103+ T cell) T cells, in the lung non-responders versus responders. This trend was not observed in the brain. Moreover, while there was no significant site-specific differences in the proportion of CD16+ CD68+ macrophages between sites alone, the lung responders had a higher proportion of this population (median=93%) compared with both brain responders (median=79.28%; p=0.0196) and brain non-responders (median=63.3%; p=0.0173) (online supplemental figure 11A–H).

The main findings regarding density and spatial distribution of T cells and macrophages in the five different anatomical sites of melanoma metastases, are summarized in table 1.

DISCUSSION

In this study, we showed that patients with melanoma with isolated metastasis to the liver, brain or bone had worse survival compared with those with lung, LN and S&S metastasis. In addition, we investigated the TIME of five different anatomical sites of melanoma metastasis in patients with untreated stage IV melanoma. We observed that liver and brain metastases were less immunogenic, that is, had fewer T cells, which were further away from melanoma cells, and reduced PD-L1 expression, particularly compared to lung and LN metastases. Liver metastases displayed significantly reduced expression of PD-1 while expressing higher levels of the immune checkpoint TIM-3 on T cells in closest proximity to melanoma cells. Both liver and lung metastases were observed to have the highest number of CD68+ macrophages, while these cells were rare in brain metastases. These findings provide insight into the differences in the TIME at different sites of metastasis and their potential impact on patient outcomes. They highlight the need for the site(s)

Table 1 Summary table of density and spatial distribution of T cells and macrophages in each site of melanoma metastasis (liver, brain, lung, subcutaneous (subcut) and lymph node

	T cell (IHC)	T cell spatial distribution	Myeloid (IHC)	Myeloid spatial distribution
Liver	∨CD3(154/mm^2) ∨PD-1 (0.7%) ∧Tim-3 (10.1%)		∧CD68	
Brain	∨CD3 (181 /mm^2) ∧PD-1 (8.9%) ∨FoxP3 (<0.5%) ∨CD103 (2.6%)	► Lowest density of CD3+ T cells within 20 µm of a melanoma cell (78 cells/ mm2)	∨CD68 ∨CD14 ∨PD-L1	► Furthest average distance between CD3+ T cells and melanoma cells (464 µm) ► Lowest density of CD68+ macrophages within 20 µm of a melanoma cell (16 cells/mm^2)
Subcut	∧CD103 (14.1%), ∧FoxP3 (3.7)	► Furthest average distance between CD3+ T cells and melanoma cells (134 µm)		
Lung	∧CD3 (436 /mm^2) ∧CD103 (12.6%), ∧Tim-3 (12.9%)	► Shortest average distance between CD3+ T cells and Melanoma cells (57 µm) ► Highest density of CD3+ T cells within 20 µm of a melanoma cell (282 cells/mm^2)	∧CD68 ∧PD-L1	► Shortest average distance between CD68+ macrophages and melanoma cells (47 µm) ► Highest density of CD68+ macrophages within 20 µm of a melanoma cell (395 cells/mm^2)
Lymph node	∧CD3 (467 /mm^2) ∧FoxP3 (3.4%) ∨Tim-3 (0.9%)			

∨=lowest expression, ∧=highest expression. Where two organ sites had similarly higher or lower expression of a particular marker both were included.
IHC, immunohistochemistry.

of melanoma metastasis to be considered when deciding potential treatment options, particularly in patients resistant to current anti-PD-1-based therapies.

Our study showed that patients with a solitary melanoma metastasis in the gastrointestinal tract have long OS in systemic therapy-naïve patients, followed by patients with melanoma metastasis in the LN and S&S. While this is an interesting finding, independent validation is needed and the underlying biology is yet to be clarified.

It has been observed previously that liver and brain melanoma metastases are associated with a poor prognosis,[22 24 25] and our data confirmed that patients with treatment-naïve melanoma with brain or liver metastases as the only site of disease had shorter OS compared with those with metastases in other sites such as the lung and LNs. In our study, we observed that metastases in the liver and brain had the lowest TIL density compared with other anatomical sites. This was consistent with data from patients with metastatic colorectal cancer, where liver metastases had reduced numbers of intratumoral TILs in comparison to distant LN metastases and to a lesser extent lung metastases.[26] The infiltration of TILs and other immune cells has previously been reported to be associated with patient prognosis in primary and metastatic melanoma, NSCLC and advanced colorectal cancer.[26–31] Our data supports the concept that the abundance of TILs in specific anatomical sites of metastasis may play a role in prognosis of patients with advanced-stage melanoma. Besides density of immune cells in the tumor microenvironment, the spatial distribution of immune cells among the tumor cells has also been reported to correlate with treatment response.[23] There is, however, a lack of research and understanding of the spatial distribution of different immune cell types compared between sites of metastasis, and whether it is associated with prognosis. Our data shows that at sites associated with a poor prognosis, such as the liver and brain, T cells were further away from melanoma cells, compared with lung and LN metastases, which are known to associate with a better prognosis. Consistent with that, lung and LNs had the highest density of CD3+ T cells within 20 µm of melanoma cells, which could suggest a higher chance of T cell-to-melanoma cell interaction.

We have described significant phenotypic differences in the T cells and macrophages present in these five anatomical sites of melanoma metastasis. Liver metastases had the lowest proportion of CD3+ T cells expressing PD-1, the primary target for anti-PD-1 therapy, while brain metastases had the highest expression of PD-1 on CD3+ T cells. This could explain why patients with liver metastases have the poorest response rates to anti-PD-1-based therapies, while patients with metastases in sites such as the brain, lung and LNs achieve higher response rates to anti-PD-1 therapy.[19 22 32] Notably, we observed higher expression of TIM-3 in liver and lung metastases, particularly on CD3+ T cells in close proximity to melanoma cells in the liver. TIM-3 functions as an immune checkpoint on T cells, which on binding with its ligand can act as a negative regulator leading to T-cell apoptosis.[33 34] Many studies suggest that an increased level of TIM-3 expression on both T cells and tumor cells is linked to poor prognosis in NSCLC, gastric cancer, colorectal and cervical cancers.[35–37] Preclinical lung cancer studies have also shown that TIM-3 can be upregulated on T cells in response to anti-PD-1-based therapies as a potential mechanism or consequence of acquired resistance. It has since been shown in murine models of colorectal and head and neck cancer that subsequent blocking of TIM-3 or combination anti-PD-L1 plus anti-TIM-3 therapy can increase response and survival.[34 38–41] These findings suggest that liver metastases' poor prognosis and/or lack of response to immunotherapy might not only be a consequence of low TIL density but also a consequence of the presence of other mechanisms of tolerance. These findings indicate that anti-PD-1 therapy alone may not be sufficient to treat liver metastases, and the addition of a TIM-3 inhibitor may potentially be a suitable therapy option for patients with liver metastases to increase response rates. Early phase clinical trials for targeting TIM-3 in various settings including as a single agent and in combination with anti-PD-L1 are currently ongoing.[33 42 43]

The innate immune system also plays a critical role in immune responses to tumors.[44] The liver, lung and brain are three organs which are known to harbor unique resident macrophage populations. Kupffer cells, liver-resident macrophages, play a role in maintaining liver homeostasis and are a first line of defense in the liver, protecting against gut bacteria, microbes and toxins that enter via the gastrointestinal tract.[45] However, in the context of liver metastases, Kupffer cells have been shown to play dual roles. During early metastatic spread Kupffer cells have been shown to play an antitumor role, increasing tumor cell death and recruitment of other inflammatory cells (eg, natural killer cells). However, they have also been shown to produce VEGF (Vascular Endothelial Growth Factor) and other growth factors promoting angiogenesis and tumor growth in later disease stages.[46] Similar to Kupffer cells in the liver, alveolar macrophages act as a first line of immune defense in the lungs while having roles in maintenance of tissue homeostasis through the removal of surfactant.[47] In the context of primary lung cancer, alveolar macrophages have also been shown to play a dual role; they have been implicated in the release of antitumoral cytokines including interleukin (IL)-1 and tumor necrosis factor-α while also producing protumoral cytokines such as IL-10, and VEGF, which promote tumor progression.[48] Our data shows that liver and lung metastases have the highest infiltration of CD68+ macrophages and being a pan-macrophage marker, this likely represents both innate resident macrophage populations and peripheral monocyte-derived macrophages that can be recruited to the site. Moreover, in this study, we did not differentiate between M1 (antitumoral) and M2 (protumoral) macrophages,[49 50] but did find a higher expression of PD-L1 on macrophages in the lung, which may contribute to the difference in response to therapy.

For a long time the brain has been considered an 'immune privileged' organ, primarily due to the function of the

blood–brain barrier (BBB) which protects brain tissue from inflammation.[51] However, the presence of metastases in the brain in and of itself represents impairment of the BBB, and thus may increase the ability of immune cells to traffic into metastatic lesions.[52 53] In this study, brain metastases were observed to have the lowest tumor infiltration of CD68+ macrophages. This could potentially be a result of either the restrictive BBB or perhaps under identifying the tissue-resident microglia populations. In contrast, melanoma mouse models have demonstrated that in the presence of both intracranial and extracranial disease, treatment with combination anti-PD-1 and anti-CTLA-4 saw a significant increase in microglia infiltration into the tumor which further correlated with treatment response.[54] Studies investigating the brain microenvironment have been particularly challenging due to the unique nature of the immune microenvironment at this site, as well as the fact it is often difficult to distinguish between, and properly characterize, microglia and monocyte-derived macrophages.[55] Further analysis of the specific macrophage populations present in the brain and other sites including liver and lung, and the role these macrophages play in the response to immunotherapy may help to improve understanding of the immune responses at specific sites of metastasis.

A limitation of this study is that we did not compare different sites of melanoma metastasis from the same patients. Multiple sites of metastasis from individual patients were not available in sufficient numbers for such a study, and we acknowledge that there is intertumoral and interpatient heterogeneity. However, to our knowledge, this is the largest study of metastatic melanoma samples across different sites of disease. Furthermore, all samples in this study were treatment-naïve and therefore our results not impacted by response/resistance to immunotherapy which may lead to changes in the immune microenvironment.[56 57] Further validation would be warranted in either an independent cohort or with the inclusion of samples obtained from multiple sites at the time of autopsy from patients with advanced melanoma.

In conclusion, this study shows that there are significant differences in the immune infiltrate within the microenvironment between sites of melanoma metastasis, not only in terms of density of immune cell types and subtypes, but also in terms of spatial distribution of these immune cells in relation to melanoma cells. While further functional testing is needed to correlate expression of these markers with clinical response to immunotherapy treatment and the underlying mechanisms and factors influencing immune cell trafficking, these findings may provide insight into site-specific response patterns to anti-PD-1-based immunotherapies. Importantly, these findings highlight organ-specific markers that could potentially be used as therapeutic targets in a personalized approach to patient treatment.

Author affiliations
[1]Melanoma Institute Australia, The University of Sydney, Sydney, New South Wales, Australia
[2]Faculty of Medicine and Health, The University of Sydney, Sydney, New South Wales, Australia
[3]Charles Perkins Centre, The University of Sydney, Sydney, New south Wales, Australia
[4]Department of Tissue Pathology and Diagnostic Oncology, Royal Prince Alfred Hospital and NSW Health Pathology, Sydney, New South Wales, Australia
[5]Westmead and Blacktown Hospitals, Sydney, New South Wales, Australia
[6]Department of Melanoma and Surgical Oncology, Royal Prince Alfred Hospital, Sydney, New South Wales, Australia
[7]Mater Hospital, Sydney, New South Wales, Australia
[8]Royal North Shore Hospital, Sydney, New South Wales, Australia
[9]Chris O'Brien Lifehouse, Camperdown, New South Wales, Australia

Twitter Richard A Scolyer @Twitter @ProfRScolyerMIA

Acknowledgements We would like to thank patients from Melanoma Institute Australia and their families for their contributions to our study. Ongoing support from colleagues at the Melanoma Institute Australia and the Charles Perkins Centre, University of Sydney, is also greatly acknowledged.

Contributors JWC and IPdS designed the study. Sample and clinical data acquisition was provided by JWC, MSC, RPMS, JFT, AJS, KFS, BS, AMM, and IPdS. Pathology was reviewed by RVR. IAV, TNG, and GHA gave guidance on experimental methods and data processing. JWC performed experiments and data analysis. MxIF panel development, thresholding, analysis and quality control undertaken by JWC and overseen by TNG, JSW, and GHA. SNL, TA, and IPdS were responsible for statistical models and analysis. Data was interpreted by JWC and IPdS. Draft manuscript prepared by JWC and IPdS. All authors reviewed and approved final manuscript. JSW, GVL, RAS, and IPdS supervised the project.

Funding This work was supported by a National Health and Medical Research Council of Australia (NHMRC) (APP1093017) Program Grant (to RAS, GVL and JFT). JWC is supported by the Emma Betts MIA PhD Scholarship and an Australian Melanoma Research Foundation (AMRF) Post-Graduate research grant. RVR is supported by a Clinical Research Scholarship from Sydney Research. GHA is supported by a scholarship from the University of Sydney and the Janet Ferguson MIA PhD Scholarship. TNG is supported by a CINSW Early Career Fellowship. RPMS is supported by Melanoma Institute Australia. AMM is supported by a NHMRC Investigator Grant, Melanoma Institute Australia and Nicholas and Helen Moore. JSW and GVL are supported by NHMRC Fellowships. GVL is also supported by the University of Sydney Medical Foundation. RAS is supported by an NHMRC (APP1141295) Practitioner Fellowship. IPS is supported by a Cancer Institute NSW Early Career Fellowship. Support from Deborah McMurtrie and John McMurtrie AM, the CLEARbridge Foundation, and the Cameron Family is also greatly acknowledged.

Competing interests MSC reports personal fees from BMS, Merck Sharp & Dohme, Novartis, Roche, Amgen, Pierre-Fabre and Ideaya. RPMS has received honoraria for advisory board participation from MSD, Novartis and Qbiotics and speaking honoraria from BMS and Novartis. JFT has received honoraria for advisory board participation from BMS Australia, MSD Australia, GSK and Provectus, and travel and conference support from GSK, Provectus and Novartis. AMM has served on advisory boards for BMS, MSD, Novartis, Roche, Pierre-Fabre and QBiotics. GVL is consultant advisor for Agenus Inc, Amgen Inc, Array Biopharma Inc, Boehringer Ingelheim International GmbH, Bristol Myers Squibb, Evaxion Biotech A/S, Hexal AG (Sandoz Company), Highlight Therapeutics S.L., Innovent Biologics USA Inc, Merck Sharpe & Dohme (Australia) Pty Limited, Merck Sharpe & Dohme, Novartis Pharma AG, OncoSec Medical Australia, PHMR Limited, Pierre Fabre, Provectus Australia, Qbiotics Group Limited, Regeneron Pharmaceuticals Inc. RAS has received fees for professional services from F. Hoffmann-La Roche, Evaxion, Provectus Biopharmaceuticals Australia, Qbiotics, Novartis, Merck Sharp & Dohme, NeraCare, Amgen, Bristol Myers Squibb, Myriad Genetics and GlaxoSmithKline. IPS had travel support by BMS and MSD, and speaker fee by Roche, Bristol Myers Squibb and Merck Sharpe & Dohme. All remaining authors declared no competing interests.

Patient consent for publication Not applicable.

Ethics approval This study involves human participants and was approved by Sydney Local Health District Human Ethics Review Committee (Protocol No. X15-0454 & HREC/11/RPAH/444 and protocol no X17-0312 & HREC/11/RPAH/32). Participants gave informed consent to participate in the study before taking part.

Provenance and peer review Not commissioned; externally peer reviewed.

Data availability statement All data relevant to the study are included in the article or uploaded as supplementary information.

ORCID iDs
Jordan W Conway http://orcid.org/0000-0003-1161-9119
Serigne Lo http://orcid.org/0000-0001-5092-5544
Grace Heloise Attrill http://orcid.org/0000-0001-8926-6582
John F Thompson http://orcid.org/0000-0002-2816-2496
Georgina V Long http://orcid.org/0000-0001-8894-3545
Richard A Scolyer http://orcid.org/0000-0002-8991-0013
Ines Pires da Silva http://orcid.org/0000-0003-3540-8906

REFERENCES

1 Eggermont AMM, Blank CU, Mandala M, *et al*. Adjuvant pembrolizumab versus placebo in resected stage III melanoma. *N Engl J Med* 2018;378:1789–801.
2 Ascierto PA, Del Vecchio M, Mandalá M, *et al*. Adjuvant nivolumab versus ipilimumab in resected stage IIIB-C and stage IV melanoma (CheckMate 238): 4-year results from a multicentre, double-blind, randomised, controlled, phase 3 trial. *Lancet Oncol* 2020;21:1465–77.
3 Robert C, Schachter J, Long GV, *et al*. Pembrolizumab versus ipilimumab in advanced melanoma. *N Engl J Med* 2015;372:2521–32.
4 Robert C, Long GV, Brady B, *et al*. Nivolumab in previously untreated melanoma without BRAF mutation. *N Engl J Med* 2015;372:320–30.
5 Larkin J, Chiarion-Sileni V, Gonzalez R, *et al*. Combined nivolumab and ipilimumab or monotherapy in untreated melanoma. *N Engl J Med* 2015;373:23–34.
6 Horn L, Mansfield AS, Szczęsna A, *et al*. First-Line Atezolizumab plus chemotherapy in extensive-stage small-cell lung cancer. *N Engl J Med* 2018;379:2220–9.
7 Gandhi L, Rodríguez-Abreu D, Gadgeel S, *et al*. Pembrolizumab plus chemotherapy in metastatic non-small-cell lung cancer. *N Engl J Med* 2018;378:2078–92.
8 Socinski MA, Jotte RM, Cappuzzo F, *et al*. Atezolizumab for first-line treatment of metastatic Nonsquamous NSCLC. *N Engl J Med* 2018;378:2288–301.
9 Robert C. A decade of immune-checkpoint inhibitors in cancer therapy. *Nat Commun* 2020;11.
10 Larkin J, Chiarion-Sileni V, Gonzalez R, *et al*. Five-Year survival with combined nivolumab and ipilimumab in advanced melanoma. *N Engl J Med* 2019;381:1535–46.
11 Imbert C, Montfort A, Fraisse M, *et al*. Resistance of melanoma to immune checkpoint inhibitors is overcome by targeting the sphingosine kinase-1. *Nat Commun* 2020;11:437.
12 Weiss SA, Wolchok JD, Sznol M. Immunotherapy of melanoma: facts and hopes. *Clin Cancer Res* 2019;25:5191–201.
13 Gide TN, Wilmott JS, Scolyer RA, *et al*. Primary and acquired resistance to immune checkpoint inhibitors in metastatic melanoma. *Clin Cancer Res* 2018;24:1260–70.
14 Gibney GT, Weiner LM, Atkins MB. Predictive biomarkers for checkpoint inhibitor-based immunotherapy. *Lancet Oncol* 2016;17:e542–51.
15 Topalian SL, Taube JM, Anders RA, *et al*. Mechanism-driven biomarkers to guide immune checkpoint blockade in cancer therapy. *Nat Rev Cancer* 2016;16:275–87.
16 Tumeh PC, Harview CL, Yearley JH, *et al*. PD-1 blockade induces responses by inhibiting adaptive immune resistance. *Nature* 2014;515:568–71.
17 Rozeman EA, Hoefsmit EP, Reijers ILM, *et al*. Survival and biomarker analyses from the OpACIN-neo and OpACIN neoadjuvant immunotherapy trials in stage III melanoma. *Nat Med* 2021;27:256–63.
18 Diem S, Kasenda B, Spain L, *et al*. Serum lactate dehydrogenase as an early marker for outcome in patients treated with anti-PD-1 therapy in metastatic melanoma. *Br J Cancer* 2016;114:256–61.
19 Pires da Silva I, Lo S, Quek C, *et al*. Site-specific response patterns, pseudoprogression, and acquired resistance in patients with melanoma treated with ipilimumab combined with anti-PD-1 therapy. *Cancer* 2020;126:86–97.
20 Tumeh PC, Hellmann MD, Hamid O, *et al*. Liver metastasis and treatment outcome with anti-PD-1 monoclonal antibody in patients with melanoma and NSCLC. *Cancer Immunol Res* 2017;5:417–24.
21 Cancer Genome Atlas Network. Genomic classification of cutaneous melanoma. *Cell* 2015;161:1681–96.
22 Vosoughi E, Lee JM, Miller JR, *et al*. Survival and clinical outcomes of patients with melanoma brain metastasis in the era of checkpoint inhibitors and targeted therapies. *BMC Cancer* 2018;18:490.
23 Gide TN, Silva IP, Quek C, *et al*. Close proximity of immune and tumor cells underlies response to anti-PD-1 based therapies in metastatic melanoma patients. *Oncoimmunology* 2020;9:1659093.
24 Waninger JJ, Ma VT, Journey S, *et al*. Validation of the American joint Committee on cancer eighth edition staging of patients with metastatic cutaneous melanoma treated with immune checkpoint inhibitors. *JAMA Netw Open* 2021;4:e210980.
25 Davies MA, Liu P, McIntyre S, *et al*. Prognostic factors for survival in melanoma patients with brain metastases. *Cancer* 2011;117:1687–96.
26 Kwak Y, Koh J, Kim D-W, *et al*. Immunoscore encompassing CD3+ and CD8+ T cell densities in distant metastasis is a robust prognostic marker for advanced colorectal cancer. *Oncotarget* 2016;7:81778-81790.
27 Fu Q, Chen N, Ge C, *et al*. Prognostic value of tumor-infiltrating lymphocytes in melanoma: a systematic review and meta-analysis. *Oncoimmunology* 2019;8:1593806.
28 Soo RA, Chen Z, Yan Teng RS, *et al*. Prognostic significance of immune cells in non-small cell lung cancer: meta-analysis. *Oncotarget* 2018;9:24801–20.
29 Sobottka B, Nowak M, Frei AL, *et al*. Establishing standardized immune phenotyping of metastatic melanoma by digital pathology. *Lab Invest* 2021;101:1561–70.
30 Schatton T, Scolyer RA, Thompson JF. *Tumor-infiltrating lymphocytes and their significance in melanoma prognosis*. Humana Press, 2014: 287–324.
31 Madore J, Strbenac D, Vilain R, *et al*. Pd-L1 negative status is associated with lower mutation burden, differential expression of immune-related genes, and worse survival in stage III melanoma. *Clin Cancer Res* 2016;22:3915–23.
32 Long GV, Atkinson V, Lo S, *et al*. Combination nivolumab and ipilimumab or nivolumab alone in melanoma brain metastases: a multicentre randomised phase 2 study. *Lancet Oncol* 2018;19:672–81.
33 He Y, Cao J, Zhao C, *et al*. TIM-3, a promising target for cancer immunotherapy. *Onco Targets Ther* 2018;11:7005–9.
34 Li H, Wu K, Tao K, *et al*. Tim-3/galectin-9 signaling pathway mediates T-cell dysfunction and predicts poor prognosis in patients with hepatitis B virus-associated hepatocellular carcinoma. *Hepatology* 2012;56:1342–51.
35 Kuai W, Xu X, Yan J, *et al*. Prognostic impact of PD-1 and Tim-3 expression in tumor tissue in stage I-III colorectal cancer. *Biomed Res Int* 2020;2020:1–13.
36 Cao Y, Zhou X, Huang X, *et al*. Tim-3 expression in cervical cancer promotes tumor metastasis 2013;8:e53834.
37 Qin S, Dong B, Yi M, *et al*. Prognostic values of Tim-3 expression in patients with solid tumors: a meta-analysis and database evaluation. *Front Oncol* 2020;10:1288.
38 Koyama S, Akbay EA, Li YY, *et al*. Adaptive resistance to therapeutic PD-1 blockade is associated with upregulation of alternative immune checkpoints. *Nat Commun* 2016;7:10501.
39 Shayan G, Srivastava R, Li J, *et al*. Adaptive resistance to anti-PD1 therapy by Tim-3 upregulation is mediated by the PI3K-Akt pathway in head and neck cancer. *Oncoimmunology* 2016;6:e1261779-e.
40 Liu F, Liu Y, Chen Z. Tim-3 expression and its role in hepatocellular carcinoma. *J Hematol Oncol* 2018;11:126.
41 Sakuishi K, Apetoh L, Sullivan JM, *et al*. Targeting Tim-3 and PD-1 pathways to reverse T cell exhaustion and restore anti-tumor immunity. *J Exp Med* 2010;207:2187–94.
42 Acharya N, Sabatos-Peyton C, Anderson AC. Tim-3 finds its place in the cancer immunotherapy landscape. *J Immunother Cancer* 2020;8:e000911.
43 Friedlaender A, Addeo A, Banna G. New emerging targets in cancer immunotherapy: the role of TIM3. *ESMO Open* 2019;4:e000497.
44 Wang H, Zhang L, Yang L, *et al*. Targeting macrophage anti-tumor activity to suppress melanoma progression. *Oncotarget* 2017;8:18486–96.
45 Krenkel O, Tacke F. Liver macrophages in tissue homeostasis and disease. *Nat Rev Immunol* 2017;17:306–21.
46 Brodt P. Role of the microenvironment in liver metastasis: from pre- to prometastatic niches. *Clin Cancer Res* 2016;22:5971–82.
47 Mukaida N, Nosaka T, Nakamoto Y, *et al*. Lung macrophages: multifunctional regulator cells for metastatic cells. *Int J Mol Sci* 2018;20:116.
48 Almatroodi SA, McDonald CF, Pouniotis DS. Alveolar macrophage polarisation in lung cancer. *Lung Cancer Int* 2014;2014:1–9.

49 Belgiovine C, Digifico E, Anfray C, *et al*. Targeting tumor-associated macrophages in anti-cancer therapies: Convincing the traitors to do the right thing. *J Clin Med* 2020;9:3226.
50 Lin Y, Xu J, Lan H. Tumor-Associated macrophages in tumor metastasis: biological roles and clinical therapeutic applications. *J Hematol Oncol* 2019;12:76.
51 Quail DF, Joyce JA. The microenvironmental landscape of brain tumors. *Cancer Cell* 2017;31:326–41.
52 Corraliza I. Recruiting specialized macrophages across the borders to restore brain functions. *Front Cell Neurosci* 2014;8:262.
53 Arvanitis CD, Ferraro GB, Jain RK. The blood-brain barrier and blood-tumour barrier in brain tumours and metastases. *Nat Rev Cancer* 2020;20:26–41.
54 Taggart D, Andreou T, Scott KJ, *et al*. Anti–PD-1/anti–CTLA-4 efficacy in melanoma brain metastases depends on extracranial disease and augmentation of CD8 $^{+}$ T cell trafficking. *Proc Natl Acad Sci U S A* 2018;115:E1540–9.
55 You H, Baluszek S, Kaminska B. Immune microenvironment of brain Metastases—Are microglia and other brain macrophages little helpers? *Frontiers in Immunology* 2019;10.
56 Zhang Y, Zhang Z. The history and advances in cancer immunotherapy: understanding the characteristics of tumor-infiltrating immune cells and their therapeutic implications. *Cell Mol Immunol* 2020;17:807–21.
57 Edwards J, Tasker A, Pires da Silva I, *et al*. Prevalence and cellular distribution of novel immune checkpoint targets across longitudinal specimens in treatment-naïve melanoma patients: implications for clinical trials. *Clin Cancer Res* 2019;25:3247–58.